Global digital elevation models for terrain morphology analysis in mountain environments: insights on Copernicus GLO-30 and ALOS AW3D30 for a large Alpine area

Sebastiano Trevisani (strevisani@iuav.it)
University IUAV of Venice
T. N. Skrypitsyna
Department of Photogrammetry, Moscow State University of Geodesy and Cartography, Moscow, Russia
I. V. Florinsky
Institute of Mathematical Problems of Biology, Keldysh Institute of Applied Mathematics, Russian Academy of Sciences

Research Article

Keywords: digital elevation model, elevation accuracy, surface roughness, terrain morphology

Posted Date: October 12th, 2022

DOI: https://doi.org/10.21203/rs.3.rs-2089787/v1

Abstract

This study focuses on the quality evaluation of two of the best 1 arc-second public global digital elevation models (DEMs), Copernicus GLO-30 DEM and ALOS AW3D30 DSM, from the perspective of their capability to represent the terrain morphology of a complex alpine landscape, located in the alpine Trentino Province, in the Italian Alps. The analysis is performed on an area of 6210 km^2, considering a reference DEM derived from a high resolution and accurate airborne Lidar DEM. The quality assessment includes, in addition to a conventional analysis of error statistics on a pixels-by-pixel basis, an ad-hoc analysis on the capability to represent the fine-scale morphology and local roughness. The quality analysis is performed considering the influence of local morphology and of the different land covers. The findings show that the two global DEMs have comparable overall quality, but the relative performances change according to local landscape characteristics. Copernicus DEM performance is on average better than ALOS in correspondence of urbanized areas as well in areas without vegetation cover, with gentle slopes and relatively low short-range roughness. ALOS DEM performance is slightly better than Copernicus in rougher terrain and steeper slopes. In general, both DEMs have poor performances in steep slopes, with a limited capability to describe correctly local morphology. The adoption of these global DEMs for terrain analysis and modelling of earth surface processes should be performed carefully, taking into account the impact of different land covers and of local morphology, including surface roughness.

1. Introduction

Global or quasi-global open-access digital elevation models (DEMs) produced from satellite data, are marked by continuous improvements in quality and accuracy (Gesch, 2018; Kakavas, Kyriou, & Nikolakopoulos, 2020; Mudd, 2020; Guth et al., 2021). The most common and popular global DEMs include versions of SRTM DEM (Farr et al., 2007), ASTER GDEM (Abrams, Crippen, & Fujisada, 2020), ALOS AW3D30 DSM (Tadono et al., 2016), MERIT DEM (Yamazaki et al., 2017), and Copernicus GLO-30 DEM (Airbus, 2020; Strobl, 2020)[1].

Global DEMs, generally more similar to digital surface models (DSMs) than to digital terrain models (DTMs), are frequently used in geoenvironmental and geoengineering studies. They have been adopted for multiple research purposes including the analysis and modeling of geoenvironmental processes related to terrain morphology more than to the overall surface morphology, which also includes anthropic structures and vegetation (Guth et al., 2021). Terrain morphology is fundamental in the context of geostructural, geomorphological, and geoenvironmental interpretation. In many applications, morphometric variables derived from DEMs are used as input features in supervised learning approaches or, at least, as proxies of other environmental variables (Wilson & Gallant, 2000; Hengl & Reuter, 2009; Florinsky, 2016, 2021; Minár, Krcho, & Evans, 2016; Trevisani & Florinsky, 2021; Trevisani et al., 2021). Examples of DEM-based studies include, but are not limited to, landslides susceptibility models (Meena & Nachappa, 2019; Titti et al., 2021), derivation of shear wave seismic velocity of shallow subsoil (Wald & Allen, 2007; Thompson, Wald, & Worden, 2014; Heath et al., 2020), derivation of drainage networks and basins with a possible adoption of ad-hoc conditioning procedures of the drainage network in

anthropized areas (Cavalli et al., 2013). Another area of DEM-based research concerns geodiversity studies, where morphometric parameters contribute to derive indexes of geodiversity (Melelli, 2014; Chrobak, Novotný, & Struś, 2021). Frequently, geodiversity studies covering large areas use global DEMs, despite the focus is on terrain morphology. DEMs are also fundamental for many processes concerning remote sensing methodologies, for example, in the context of SAR interferometry technology in the study of ground displacements (Bayer, Schmidt, & Simoni, 2017).

Given the importance of global DEMs (Schumann & Bates, 2018), it is not surprising that the wide set of studies concerning the quality and accuracy of these digital products (Purinton & Bookhagen, 2017; Rizzoli et al., 2017; Boulton and Stokes, 2018; Caglar et al., 2018; Florinsky, Skrypitsyna, & Luschikova, 2018; Gonzalez & Rizzoli, 2018; Grohmann, 2018; Jain et al., 2018; Li & Zhao, 2018; Florinsky et al., 2019; Liu et al., 2019; González-Moradas & Viveen, 2020; Kakavas, Kyriou, & Nikolakopoulos, 2020; Vassilaki & Stamos, 2020; Mesa-Mingorance & Ariza-López, 2020; Guth & Geoffroy, 2021), including the recent DEMIX initiative (Strobl et al., 2021) aimed to develop a participative and standardized approach for global DEMs quality evaluation. Most of the studies generally focus on the evaluation of the inherent quality of DEMs products considering a reference DEM or a set of ground control points (Guth et al., 2021). However, as noted above, for geoengineering and geoenvironmental applications, it is fundamental to understand the capability and quality of global DEMs from the viewpoint of their capability to describe terrain morphology, possibly considering different land covers and morphological settings. In fact, in areas with dense vegetation and anthropic structures, the capability of global DEMs to reproduce terrain morphology is mainly influenced by the land cover characteristics, while in other areas it is mainly affected by the characteristics of local morphology, such as slope and surface roughness.

The capability of a DEM to reproduce terrain morphology cannot be fully captured by the statistical analysis of pixel-by-pixel differences respect to a reference DEM, adopting conventional metrics such as root mean square error (RMSE), mean/median error and mean/median absolute error (e.g., Florinsky et al., 2019; Crema et al. 2020; Polidori & El Hage, 2020). Differently, the spatial variability structure (Isaaks & Srivastava, 1989) of DEMs should be considered in the evaluation of their quality, for example including the capability to reproduce fine-scale morphology and different aspects of surface roughness (e.g., Trevisani, Cavalli, & Marchi, 2012). The necessity to move beyond the evaluation of error statistics on a pixel-by-pixels basis is advocated also in the analogous context of image analysis. From this perspective, the structural similarity index (Wang et al., 2004; Crema et al., 2020) could be mentioned, since it considers the spatial variability structure in evaluating the similarity between a sample image and a reference one.

Accordingly, this research focuses on the quality evaluation of two of the best 1 arc-second public global digital elevation models, Copernicus GLO-30 version 2021_1 (hereinafter referred to as COP) (Airbus, 2020; Strobl, 2020) and ALOS AW3D30 version 3.2 (hereinafter referred to as ALOS) (JAXA, 2021a, 2021b), from the perspective of their capability to represent the terrain morphology of a complex alpine landscape, located in the alpine Trentino Province (Italian Alps). The analysis, following a previous study (Florinsky et al., 2019) concerning the quality evaluation of several global DEMs in the same area, is

conducted considering a reference DEM (herewith referred to as reference) derived from the upscaling of an accurate and high-resolution airborne Lidar DEM (Cavalli et al., 2013; Portale cartografico, 2016). The study area is well suited for an analysis of this kind for several reasons: 1) large extent, approximately 6210 km^2; 2) high heterogeneity in morphology and land cover; 3) demanding morphological conditions for the remote sensing technologies adopted for the derivation of the global DEMs; 4) public availability of reference DEMs with creative common license (Portale cartografico, 2016).

The two global DEMs are considered among the best freely available global DEMs at 1 arc-second resolution. On the one hand, COP version 2021_1 seems particularly promising (Guth & Geoffroy, 2021) with remarkable improvements respect to the older EU-DEM version 1.1 (Bashfield & Keim, 2011). On the other hand, ALOS resulted the one with the best performances in the previous study conducted in the Alpine area (Florinsky et al., 2019) as well as in other regions (Caglar et al., 2018; Florinky, Skrypitsyna, & Luschikova, 2018; Jain et al., 2018; Li & Zhao, 2018; Liu et al., 2019; González-Moradas & Viveen, 2020). The quantitative analysis of the DEMs quality is performed both in terms of conventional error statistics computed on a pixel-by-pixel basis as well as from the perspective of the capability to represent the spatial variability structure (i.e., roughness) of the local surface morphology. Moreover, the analysis is performed considering specific land cover types and morphological settings, permitting to evaluate the capability of the two global DEMs to reproduce terrain morphology in different land cover and morphological settings.

[1] In this article, we use the term DEM according to its definition given by Guth et al. (2021): '*DEM (digital elevation model): General term for a digital representation of elevations (or height) of a topographic surface in form of a georectified point-based or area-based grid, covering the Earth or other solid celestial bodies*'. According to other definitions reported in Guth et al. (2021), the listed global DEMs are more similar to digital surface models (DSMs), that is, DEMs comprising buildings and vegetation, rather than to digital terrain models (DTMs), that is, DEMs with buildings and vegetation cover removed ('bare-earth' DEMs).

2. Study Area

The study area is the Autonomous Province of Trento, in the northeastern Alps, with an extent of 6210 km^2 (Fig. 1). The morphology of the province is heterogeneous, also in relation to the complexity of the geostructural setting (Castellarin et al., 2005), with elevations ranging from 65 m to 3760 m above sea level, with approximately the 70% of the area lying above 1000 m. Forests cover approximately 60% of the area, while rocky outcrops occupy about 7% of the territory. Flat and gentle slopes are intensely anthropized, including urban areas and agricultural land, covering approximately the 19% of the territory. Lakes and glaciers cover minor proportions of the landscape (Cavalli et al., 2013).

3. Materials And Methods

3.1. Global DEMs

For the study area, ALOS AW3D30 DSM version 3.2 (JAXA, 2021a) and Copernicus GLO-30 DEM version 2021_1 (ESA, 2021) have been downloaded and cropped according to the study area extent.

The ALOS AW3D30 DSM is a photogrammetric DEM derived from visible-band stereo images with a 2.5 m resolution acquired by the ALOS spacecraft in 2006–2011 (Tadono et al., 2016; Takaku et al., 2016; Takaku & Tadono, 2017). ALOS AW3D30 DSM versions 1.1 and 2.1 became respectively available in 2016 and 2018 (JAXA, 2021a) at a resolution of 1 arc-second (approximately 30 m at the equator, and 26 m at the considered latitude, in EW direction) and a specification accuracy (rms) of 5 m (Takaku & Tadono, 2017). Further versions have been then released with quality improvements in northern and southern regions. In the high-latitude regions, different pixel spacing was adopted for each latitude zone. Regarding auxiliary data, coastlines were updated using new auxiliary data and removing incorrect sea masks over land. The anomaly detection algorithm has been improved and the anomalies were partially corrected with new additional data (JAXA, 2021b).

The Copernicus GLO-30 DEM at a resolution of 1 arc-second was obtained by resampling the original, 12 m-gridded WorldDEM™ (Airbus, 2020; Strobl, 2020). The WorldDEM™ has been derived from radar interferometry data (X-band) obtained during the TanDEM-X mission in 2011–2015, with a first release in 2019 (Rizzoli et al., 2017). The declared absolute vertical accuracy is approximately 4 m (90% linear error), the relative vertical accuracy is approximately 2 m for slopes $\leq$ 20%, and 4 m for slopes > 20%. The WorldDEM™ has been edited applying various filters and filling gaps using data from other global DEMs (Airbus, 2020). In the studied spatial domain, the Copernicus DEM is characterized by several void filled areas resolved with a wide set of procedures and alternative DEMs (Fig. 2).

COP and ALOS DEMs have been projected in WGS 84 UTM 32N at a resolution of 25 m, according to a grid based on the reference DEM, using bilinear interpolation for the alignment (using Esri - ArcMap 10.8.1. GIS). The decision to perform the analysis in a projected system is dictated by the fact that in most geoenvironmental applications, at the local and regional level (e.g., landslide susceptibility mapping, flood analysis, landslide runout modeling, etc.), are conducted on projected coordinate systems and not in geographical ones. Accordingly, it is of interest to evaluate the quality of the global DEMs after the projection and alignment on a common grid system. Moreover, the alignment on the reference grid is convenient, considering that ALOS and COP have a different grid coding system, inducing a shift of half pixel between the two (Guth et al., 2021). It is worth noting that the projection induces some degradation of the original quality of global DEMs; however, the error induced by the process is not marked and the impact on the statistical distribution of DEM differences is low. For providing an empirical evaluation of the impact of projection, for a subset of the study area with an extent of approximately 12 km × 10 km, an alternative procedure for evaluating the differences between COP and the reference has been tested. The alternative procedure maintains unaltered the COP coordinate system and grid geometry, hence preserving original pixel values and accuracy. Differently the reference DEM is derived according to the COP grid, upscaling the reference DEM at 2 m resolution, computing the average elevation of pixels comprised in each pixel of COP. The two procedures provide a comparable statistical distribution in elevation differences between COP and the reference. With the approach adopted in this study, the

differences are slightly higher, with an increase of 5% for the median absolute differences and of 1.5% for the RMSE.

The elevation of COP is expressed according to the geoid EGM2008 (Pavlis et al., 2012), which is similar to the local geoid adopted in the Trentino Province. The geoid EGM2008 has been selected as the common potential gravimetric surface for the DEMs considered in this study. The elevations of ALOS are expressed according to EGM96 (Tadono et al., 2016), less accurate and with lower spatial resolution than EGM2008 and the local geoid adopted by the Trento Province. The transformation of the elevations of ALOS from EGM96 to EGM2008 has been conducted considering the EGM96 deviations derived from the 360 spherical harmonics components (code and data are available from https://earth-info.nga.mil/) and the EGM2008 geoid grid with a 1 arc-minutes resolution.

3.2. Reference DEM

The reference DEM at a 25 m resolution has been derived from high resolution DTMs obtained by means of airborne Lidar scanning (Cavalli et al., 2013). The Lidar survey has been conducted between 2006 and 2008 covering the Trentino Province (Portale geocartografico, 2016). The DTMs have a resolution of 1 m and a reported vertical accuracy of 15 cm in valleys and urbanized areas; in the remaining areas the resolution is of 2 m with a reported vertical accuracy of 30 cm. The reference DEM at a resolution of 25 m has been generated by upscaling the original DEM resolution by cell aggregation using the mean as estimator. To perform this operation the function “Aggregate” of the Arcmap10.8.1 Spatial Analyst extension has been deployed. Accordingly, the pixels values of the reference DEM represent elevation values with a spatial support of 25 m · 25 m. As reported in the previous study (Florinsky et al., 2019), an indicative assessment of the accuracy of the upscaled reference DEM has been performed considering 111 ground control points, pertaining to a 4th-order regional geodetic network, stationed with satellite receivers using static or rapid-static techniques (Servizio catasto di Trento, 2011; Chistè, Nardelli, & Sevegnani, 2013). The resulting mean error is of -2.14 m with a standard deviation of 3.5 m; the error can be considered relatively low, considering that the ground control points have a punctual spatial support (often located on peaks), and the elevations of the reference DEM are representative of the mean elevation of a 25 m · 25 m area.

The reference DEM elevations are expressed respect to a local geoid (Di Girolamo, 2008) adopted for the topographic and cadastral services of the Trentino Province. The elevations have been transformed to the common geoid EGM2008, using the local geoid grid and the EGM2008 at 1 arc-minute resolution. From the tests performed on thousands of ground control points (Chistè, Nardelli, & Sevegnani, 2013), located mainly on structures, the interpolated local geoid is quite accurate, with a standard deviation of 0.2 m. Moreover, the differences between EGM2008 and the local geoid are not marked, with a mean difference of 0.47 m and a standard deviation of 0.07 m.

3.3. Data analysis

The statistical and spatial-statistical analysis of the differences between the global DEMs and the reference have been conducted using various software including proprietary geographic information systems (ESRI ArcMap 10.8.1 and MapInfo) and an open-source solution based on the Terra package (Hijmans et al., 2022) in the R statistical computing environment (R Foundation, 2022). ArcMap 10.8.1 has been deployed for visual analysis, creation of maps, and cross-checking of some of the results obtained in R. The basic statistical functions of R and the possibility to manipulate raster data provided by the Terra package have been deployed for computing the statistical metrics and statistical graphs. Standard statistical indexes have been used for characterizing the statistical distribution of differences and absolute differences in elevation, computed pixel-by-pixel between the global DEMs and the reference: mean, median, standard deviation, RMSE, and quantiles. The Corine 2006 (CLC2006) land cover map (EEA, 2020) has been adopted for stratifying the analysis according to land cover typologies, being derived in the same period of the survey of the reference DEM. It should be considered that CLC2006 has a minimum mapping unit of 25 ha and, accordingly, some noise due to misclassification should be expected considering the higher resolution of the DEMs. Nevertheless, as confirmed also by means of the visual analysis of orthomosaics (pixel size of 1 m), the accuracy and resolution of CLC2006 permit to differentiate appropriately, for the intended tasks of this study, the different land covers in the area. Considering the characteristics of the area and the study aims, the CLC2006 has been reclassified grouping the original classes in a lower number, generating the following classes: 'Agriculture' (areas dedicated to agriculture), 'Forest' (dense vegetation cover), 'Forest (Low)' (transitional woodland-shrub), 'Grasslands' (mainly pastures and natural grasslands), 'Outcrop' (bare rock and shallow bedrock), 'Urban' (anthropized areas). The proportion of the considered landcovers in the area are: 'Agriculture' 10.2%, 'Forest' 55.8%, 'Forest (low)' 6%, 'Grassland' 17.4%, 'Outcrop' 7%, 'Urban' 2.8%.

In addition to the usual statistics for the evaluation of DEM differences on a pixel-by-pixels basis, metrics outlining the capability to reproduce fine-scale morphology have been considered. The calculations have been mainly performed using focal functions of the Terra package and the R standard statistical functions; ArcMap algorithms deploying Spatial Analyst focal functions (Trevisani & Rocca, 2015) have been adopted for cross-checking the results obtained in R. Spatial-statistical indexes capable to provide information on local surface spatial-variability have been adopted (Trevisani, Cavalli, & Marchi, 2012). The methodology relies on a geostatistical-based approach for surface roughness analysis (Trevisani & Rocca, 2015; Trevisani & Cavalli, 2016). The roughness metrics are derived by means of local measures of spatial variability computed on a detrended version of the DEM (i.e., residual DEM).

A residual DEM is obtained by means of a high pass filter (e.g., Wilson and Gallant, 2000; Hiller & Smith, 2008; Florinsky, 2016) removing large-scale variations (i.e., a smoothed DEM) from the original DEM. The residual DEM permits to compute local roughness indexes that are not influenced by local slope. In this study, the residual DEMs have been derived subtracting from the original DEMs a smoothed DEM obtained via a simple single-pass moving average approach, using a circular moving window with a radius of 3 pixels (i.e., covering 29 pixels). The residual DEM highlights fine-scale morphologies including potential artifacts (Fig. 3), and it is fundamental for the calculation of the roughness index considered (Fig. 3c), even if solutions bypassing DEM trending are available (e.g., Trevisani et al., 2022). Moreover,

the analysis of the correlation (Pearson) between the residual global DEMs and the residual reference provides an immediate index reporting the capability to reproduce fine-scale morphology.

The study focuses on a specific aspect of surface roughness, the short-range isotropic roughness, computed by means of the geostatistical algorithm based on MAD estimator (Eq. 1), proposed by Trevisani & Rocca (2015) for the analysis of geomorphometric data, as an improvement of the variogram (Eq. 2) or its generalization (Eq. 3) (e.g., Isaaks & Srivastava, 1989):

$$\mathrm{MAD}(\boldsymbol{h}) = |\Delta(\boldsymbol{h})_{\alpha=median}| \quad (1)$$

$$\gamma(\boldsymbol{h}) = \frac{1}{2\mathrm{N}(\mathbf{h})}\sum_{\alpha=1}^{N(\boldsymbol{h})}[z(\boldsymbol{u}_\alpha) - z(\boldsymbol{u}_\alpha + \boldsymbol{h})]^2 = \frac{1}{2N(\boldsymbol{h})}\sum_{\alpha=1}^{N(\boldsymbol{h})}\Delta^2(\boldsymbol{h})_\alpha = \frac{1}{2}\cdot \mathrm{mean}(\Delta^2(\boldsymbol{h})) \quad (2)$$

$$\gamma(\boldsymbol{h})_p = \frac{1}{2\mathrm{N}(\mathbf{h})}\sum_{\alpha=1}^{N(\boldsymbol{h})}|z(\boldsymbol{u}_\alpha) - z(\boldsymbol{u}_\alpha + \boldsymbol{h})|^p = \frac{1}{2}\cdot \mathrm{mean}(|\Delta(\boldsymbol{h})|^p) \quad (3)$$

$$\text{with } \Delta(\boldsymbol{h})_\alpha = z(\boldsymbol{u}_\alpha) - z(\boldsymbol{u}_\alpha + \boldsymbol{h}),$$

In Eqs. (1–3), h is the separation vector (lag) between two locations (u), z(u) is the value of the variable of interest in the location u (e.g., residual elevation), and *N*(h) is the number of point pairs separated by h found in the search window. While the variogram (Eq. 2, or Eq. 3 with $p = 2$) and the madogram (Eq. 3 with $p = 1$) use as estimator of spatial variability the mean, MAD adopts the median, resulting in estimator less sensitive to data contamination. For a given search window, MAD reports the median absolute difference in residual elevation between pixels separated by a given lag distance and for a given direction. Calculating the indexes for different values of h it is possible to derive a multiscale and directional characterization of surface roughness.

In this study, a simple short-range isotropic (i.e. omnidirectional) index was calculated considering a lag distance of 2 pixels in any direction and with a circular search window with a radius of 3 pixels. The short-range isotropic roughness index considered, focusing on short-range spatial variability, provides an intuitive index of the capability of global DEMs to reproduce fine-scale terrain roughness. This roughness index was chosen for its simplicity and high informativeness; however, it is worth noting that other estimators can be considered, for example tailored to the detection of artifacts in DEMs. From this perspective, variogram and madogram (Eqs. 2 and 3) would permit to highlight anomalous data, being these estimators more sensitive to outliers; however, the general description of surface roughness would appear blurred, given the heterogeneity in roughness of the studied terrain (see Trevisani and Rocca, 2015). Moreover, other aspects and scales of surface roughness could be analyzed (e.g., roughness anisotropy, Trevisani et al. 2012).

4. Results And Discussion

4.1. DEM differences statistics

The statistical distribution of differences between the global DEMs and the reference (Fig. 4 and Table 1), computed considering all land cover typologies, reveal a higher positive bias and a higher dispersion of differences for COP than for ALOS. Even regarding absolute differences, COP is characterized by higher median error, mean error, and RMSE. However, when focusing on areas without vegetation and anthropic structures, i.e., “Outcrop” and “Grassland” land covers, the situation reverts, and COP shows better performances than ALOS, in terms of median differences and median absolute differences. The analysis of differences for “Outcrop” and “Grassland” land covers provides information on the inherent quality of Global DEMs, at least when adopting robust statistics such as the median, in order to reduce the impact of noise due to landcover misclassifications. It is evident (Fig. 4 and Table 1) that in these land covers, COP is better than ALOS both in terms of median error as well as of median absolute error. ALOS shows a wider variability and in general a negative bias. This is particularly evident in the “Low Forest” and “Agriculture” land covers (Fig. 4), with negative values of the first quartile, unexpected given the presence of vegetation. In general, COP is characterized by larger positive median differences for forested areas respect to ALOS. In “Urban” land cover the median differences are similar, but ALOS has a higher dispersion of differences.

Table 1
Statistics of the differences and absolute differences between global DEMs and the reference for different landcovers typologies (all land covers, “Grassland” and “Outcrop”).

Landcover	**DEM-Reference (m)**	**1st Qu. (m)**	**Median (m)**	**Mean (m)**	**3rd Qu. (m)**
All	COP (RMSE 16.09 m)	0.66	5.94	7.64	14.25
	ALOS (RMSE 14.01 m)	-0.31	3.86	5.36	11.09
Outcrop	COP (RMSE 27.60 m)	-3.24	-0.35	-3.41	1.83
	ALOS (RMSE 27.89 m)	-5.86	-2.17	-3.62	1.41
Grassland	COP (RMSE 13.52 m)	-1.08	0.37	1.37	2.5
	ALOS (RMSE 11.96 m)	-3.78	-0.89	-0.78	1.84
Landcover	**|DEM-Reference| (m)**	**1st Qu. (m)**	**Median (m)**	**Mean (m)**	**3rd Qu. (m)**
All	COP	1.88	7.1	10.06	14.96
	ALOS	2.06	5.45	8.34	11.94
Outcrop	COP	0.95	2.45	10.48	8.26
	ALOS	1.89	4.2	10.14	8.37
Grassland	COP	0.69	1.72	5.11	4.27
	ALOS	1.29	2.92	5.31	5.68

As expected, the differences between the global and reference DEMs are strongly influenced by the land cover type (Fig. 4), with reflections also on the capability to represent fine-scale terrain morphology, as described in the next section. Given the statistics, the use of the global DEMs in forested areas should be performed carefully, especially when the purpose is the modeling of surface flow processes or the derivation of terrain morphometric variables.

It is also interesting to analyze the relation between the DEMs differences statistics and local morphology, in terms of local slope and short-range roughness (Figs. 5–7). Accordingly, the statistical metrics of DEMs differences have been calculated stratifying the data in relation to classes of slope (class interval of 2.5°) and isotropic short-range roughness (class interval of 1 m), computing the slope and roughness on the reference DEM. For each combination of slope-roughness classes, the following statistics have been calculated (considering a minimum of 50 data): number of data (i.e., pixels), mean slope of the reference, mean roughness of the reference, RMSE for COP, RMSE for ALOS, correlation between the residual global DEMs and the residual reference. Limiting the analysis to “Grassland” and “Outcrop” land covers (Fig. 5–6), it is possible to focus on the influence of local morphological setting on the differences between global DEMs and the reference. As general tendency (Fig. 6), COP outperforms ALOS in areas with slopes lower than 40° and a relatively smooth topography. Differently, considering all land covers (Fig. 7), this behavior is not observed, being the statistical distribution of differences mostly influenced by land covers.

Limiting the analysis to “Grassland” and “Outcrop” land covers, it is interesting to analyze in more details the differences between global DEMs and the reference, considering areas with gentle slopes and low local roughness. These settings are comparable to those adopted in the usual statistical performance tests of the global DEMs, which consider mainly flat areas (e.g., Caglar et al., 2018). Limiting the analysis to slopes lower than 5° (for a statistical distribution of slopes see Table 2) in any condition of local roughness, the RMSE of COP and ALOS is 4.54 m and 5.11 m respectively. Differently, considering areas with a short-range roughness less than 1.3 m, corresponding to the median value of roughness in that slope range, the RMSE of COP and ALOS is 1.86 m and 2.62 m respectively.

Table 2
Quantiles of slope distribution for the study area, calculated from the reference

Quantiles	0%	10%	20%	30%	40%	50%	60%	70%	80%	90%	100%
Slope	0°	7.6°	13.5°	18.4°	22.7°	26.5°	30.1°	33.4°	37°	42.5°	84.2°

It is worth noting that the impact of local roughness on error is significant also in correspondence of mild and steep slopes. Up to slopes of approximately 40°, COP outperforms ALOS in areas with relatively smooth topography, up to values of isotropic short-range roughness of approximately 8 m. For example, considering slopes between 30° and 35° in terrains with roughness values less than the median value of

roughness (3.72 m) for that slope range, the RMSE of COP and ALOS is 4.86 m and 7.13 m respectively. Above the roughness threshold, the RMSE of COP and ALOS is 15.85 m and 14.85 m respectively.

At steeper slopes the accuracy of the ALOS and COP are comparable with slightly better performances of the former. For example, considering slopes between 50° and 55° in terrains with roughness values less than the median value of roughness (9.98 m), the RMSE of COP and ALOS is 22.5 m and 20.22 m respectively. Above that roughness threshold, the RMSE of COP and ALOS is 48.44 m and 46.09 m respectively. Anyway, at these very steep slopes the differences in accuracy between the two global DEMs are erratic, and it is not feasible to individuate a clear pattern, partly in relation to the low amount of data in this slope range (Table 2) and also due to the interpolation error.

A further appreciation of the differences between the global and reference DEMs can be provided analyzing the spatial distribution of differences in specific areas (Fig. 8). As confirmed by the statistics, in areas without vegetation cover and anthropic structures, the differences between COP and the reference are not biased, while ALOS tends to have a negative bias, except for some areas with positive errors. A similar trend was observed for other European regions (Florinsky, Skrypitsyna, & Luschikova, 2018). In “Grassland” and “Outcrops” land covers, the variability of errors for COP seems lower than for ALOS. In urban areas, the patterns of positive errors of COP resemble the spatial patterns of anthropic structures and agriculture fields; differently, for ALOS the spatial distribution of differences seems less spatially structured. These characteristics, as discussed in the next section, are then confirmed by the analysis of the correlation between residual DEMs and by the capability to reproduce short-range roughness.

4.2. Quality in reproducing terrain morphology

The visual comparison of the residual global DEMs (Fig. 9) with the residual reference DEM highlights the poor capability to describe fine-scale morphology and the presence of various artifacts. A quantitative evaluation of the capability to represent fine-scale morphology is achieved considering the correlation coefficient (Pearson) between the residual global DEMs and the residual reference DEM (Table 3 and Fig. 10). In general, considering all morphological settings and land covers, ALOS tends to show higher correlation than COP, even if it is characterized by the presence of various artifacts. Looking at the different land covers, marked differences between the two global DEMs are in correspondence of “Outcrops”, “Grassland” and “Forest” land covers. Differently, the performance is comparable for “Agriculture” and “Urban” land covers, with the last one characterized by a slightly better performance of COP.

Table 3
Correlation between residual global DEMs and the residual reference, for different land covers

Landcover	Residual DEM	Correlation
All	COP	0.65
All	ALOS	0.72
Outcrop	COP	0.53
Outcrop	ALOS	0.6
Grassland	COP	0.65
Grassland	ALOS	0.72
Forest	COP	0.68
Forest	ALOS	0.76
Agriculture	COP	0.77
Agriculture	ALOS	0.79
Urban	COP	0.66
Urban	ALOS	0.65

Focusing on “Outcrop” and “Grassland” land covers, it is possible to analyze better as the correlation between the residual DEMs (Fig. 10) changes according to the morphological characteristics, considering both slope and roughness. From the analysis, it is evident how the performances are influenced by the morphological setting, as already seen for the RMSE (Figs. 6 and 7). COP outperforms ALOS in areas with low/moderate slopes (e.g., slope less than 35° – 40°) and a relatively smooth surface (e.g., short-range roughness less than 8 m). ALOS has better performances with steeper slopes (up to 55°–60°) and higher short-range roughness.

These aspects can be further investigated evaluating the capability of COP and ALOS to represent short-range surface roughness (Figs. 11–13), considering the ratio of the roughness computed from the Global DEM to the roughness computed from the reference. Both COP and ALOS smooth severely short-range surface roughness, and the smoothing changes in function of the different land covers and local slope (Fig. 11). This suggest that the real spatial support of measurement (Isaaks & Srivastava 1989; Burrough & McDonnell 1998) is much larger than 1 arc-second. COP, apart from “Urban” land cover, tends to smooth with all land covers, with an overall median reduction of short-range roughness up to 29%; ALOS is characterized by a lower level of smoothing, with a median reduction of 17%. However, these values should be interpreted carefully, being related to multiple factors including land cover, morphological setting, and the presence of artifacts. Focusing on “Grassland” and “Outcrops” land covers (Fig. 11), it is evident a drop in the roughness ratios in correspondence of slopes steeper than 45°. ALOS behaves a

little differently, with also “Agriculture” land cover, in addition to “Urban” one, presenting tendentially higher roughness. The smoothing of ALOS seems tendentially less severe than for COP, but this is partly due to the presence of artifacts (e.g., red boxes in Figs. 12–14) that contribute to increase local roughness.

The differences between COP and ALOS in their capability to reproduce terrain fine-scale morphology in the different morphological and land cover settings are justified by the different technology and methodology adopted for deriving these global DEMs. In fact, the specifics of signal acquisition and processing are of critical importance in the creation of the surface model. Even though attempts have been made to correct implausible values, high-altitude peaks in rugged terrain and/or with snow cover are still a challenge for terrain modeling (e.g., red box and arrows in Figs. 12 and 14), both with the data obtained by radar imaging as well as by optical range imaging. Frequently, the radar surveying on high, rugged, and snowy terrain is characterized by information gaps and void filling algorithms are applied. In the same terrains, photogrammetric processing of images generates artifacts caused by correlation errors. In urban areas (Fig. 13), the lower performance of ALOS respect to COP are likely caused by the interpolation of the photogrammetric point cloud without prior filtering of structures and vegetation. Finally, the stripy artifacts of ALOS (Figs. 13 and 14) are also related to the integer representation of elevation values. Other examples of artifacts in ALOS, and, to a minor extent, in COP are presented in Fig. 14. Regarding ALOS, depressions and bumps are particularly evident and are likely related to correlation errors due to perspective distortions of the slopes, their varying conditions of illumination and, in some circumstances, presence of snow.

5. Conclusions

In the large Alpine area considered it is difficult to assess which of the two global DEMs, COP or ALOS, is the best from the perspective of terrain morphology representation. In fact, the relative performances are dependent on land covers and local morphological settings. COP has on average better performances in areas with low/mild slopes (up to 35°– 40°) and relatively low short-range roughness, especially in urbanized valleys and grasslands, with a relatively gentle morphology. ALOS shows slightly better performances in more rugged terrain and steeper slopes (up to 55°–60°). In general, with steep slopes, rugged morphology and/or forested land covers both DEMs have poor performances in reproducing terrain morphology. The analysis of short-range roughness permitted to highlight peculiar aspects on the quality of these DEMs, and it represents a relevant morphological factor, in conjunction with slope, influencing the accuracy of the DEMs. COP tends to smooth more severely short-range roughness compared to ALOS. However, ALOS is in some areas characterized by different types of artifacts. Finally, the analysis of residual DEMs and of the short-range roughness suggest that the true spatial resolution of these global DEMs is lower respect to their grid spacing and some level of upscaling may be required for their proper use.

References

1. Abrams, M., Crippen, R., & Fujisada, H. (2020). ASTER global digital elevation model (GDEM) and ASTER global water body dataset (ASTWBD). *Remote Sensing,* 12, 1156. doi:10.3390/rs12071156.
2. Airbus (2020). *Copernicus DEM: Copernicus digital elevation model product handbook. Report AO/1-9422/18/I-LG*. Taufkirchen, Germany: Airbus Defence and Space GmbH.
3. Bashfield, A., & Keim, A. (2011). Continent-wide DEM creation for the European Union. In *34th International Symposium on Remote Sensing of Environment, Sydney, Australia, 10–15 April 2011*.
4. Bayer, B., Schmidt, D., & Simoni, A. (2017). The influence of external digital elevation models on PS-InSAR and SBAS results: implications for the analysis of deformation signals caused by slow moving landslides in the Northern Apennines (Italy). *IEEE Transactions on Geoscience and Remote Sensing,* 55, 2618–2631. doi:10.1109/TGRS.2017.2648885.
5. Boulton, S. J., & Stokes, M. (2018). Which DEM is best for analyzing fluvial landscape development in mountainous terrains? *Geomorphology* 310, 168–187. doi:10.1016/J.GEOMORPH.2018.03.002.
6. Burrough, P. A., & McDonnell, R. A. (1998). *Principles of geographical information systems*. 2nd ed. Oxford: Oxford University Press.
7. Caglar B., Becek, K., Mekik, C., & Ozendi, M. (2018). On the vertical accuracy of the ALOS World 3D-30m digital elevation model. *Remote Sensing Letters,* 9, 607–615. doi:10.1080/2150704X.2018.1453174.
8. Castellarin, A., Dal Piaz, G. V., Picotti, V., Selli, L., Cantelli, L., Martin, S., Montresor, L., & Nardin, M. (2005). *Note illustrative della carta geologica d'Italia alla scala 1:50,000, foglio 059 'Tione di Trento'*. Trento, Italy: APAT and Dipartimento Difesa Del Suolo – Servizio Geologico D'Italia.
9. Cavalli, M., Trevisani, S., Goldin, B., Mion, E., Crema, S., & Valentinotti, R. (2013). Semi-automatic derivation of channel network from a high-resolution DTM: the example of an Italian Alpine Region. *European Journal of Remote Sensing,* 46, 152–174. doi:10.5721/EuJRS20134609.
10. Chrobak, A., Novotný, J., & Struś, P. (2021). Geodiversity assessment as a first step in designating areas of geotourism potential. Case study: Western Carpathians. *Frontiers in Earth Science,* 9, 752669. doi:10.3389/feart.2021.752669.
11. Crema, S., Llena, M., Calsamiglia, A., Estrany, J., Marchi, L., Vericat, D., & Cavalli, M. (2020). Can inpainting improve digital terrain analysis? Comparing techniques for void filling, surface reconstruction and geomorphometric analyses. *Earth Surface Processes and Landforms,* 45, 736–755. doi:10.1002/esp.4739.
12. Chistè, F., Nardelli, C., & Sevegnani, D. (2013). MobileKat "Public Utility" per la localizzazione dei punti fiduciali catastali". In *Atti 17a Conferenza Nazionale delle Associazioni Scientifiche per le Informazioni Territoriali e Ambientali (ASITA), Riva del Garda, Italy, 5–7 Nov. 2013*. 449–453.
13. Di Girolamo, A. (2008). *Le quote dei punti determinate con GPS. Variazioni locali degli scostamenti geoidici in Trentino Alto Adige*. Technical report. Bolzano, Italy: Ufficio per il Rilevamento Geodetico – Regione Autonoma Trentino Alto Adige.
14. EEA (2020). *Corine land cover (CLC) 2006, version 2020_20u1*. European Environment Agency (EEA), Copernicus Program. https://land.copernicus.eu/pan-european/corine-land-cover.

15. ESA (2021). *Copernicus space component data access PANDA catalogue*. European Space Agency. https://panda.copernicus.eu/web/cds-catalogue/panda.
16. Farr, T. G., Rosen, P. A., Caro, E., Crippen, R., Duren, R., Hensley, S., Kobrick, M., et al. (2007). The Shuttle radar topography mission. *Reviews of Geophysics,* 45, RG2004. doi:10.1029/2005RG000183.
17. Florinsky, I. V. (2016). *Digital terrain analysis in soil science and geology*. 2nd ed. Amsterdam, the Netherlands: Elsevier / Academic Press.
18. Florinsky, I. V. (2021). Geomorphometry today. *InterCarto. InterGIS,* 27, 2, 394–448 (in Russian, with English abstract). doi:10.35595/2414-9179-2021-2-27-394-448.
19. Florinsky, I. V., Skrypitsyna, T. N., & Luschikova, O. S. (2018). Comparative accuracy of the AW3D30 DSM, ASTER GDEM, and SRTM1 DEM: A case study on the Zaoksky Testing Ground, Central European Russia. *Remote Sensing Letters,* 9, 706–714. doi:10.1080/2150704X.2018.1468098.
20. Florinsky, I. V., Skrypitsyna, T. N., Trevisani, S., & Romaikin, S. V. (2019). Statistical and visual quality assessment of nearly-global and continental digital elevation models of Trentino, Italy. *Remote Sensing Letters,* 10, 726–735. doi:10.1080/2150704X.2019.1602790.
21. Gesch, D. B. (2018). Best practices for elevation-based assessments of sea-level rise and coastal flooding exposure. *Frontiers in Earth Science,* 6, 230. doi:10.3389/feart.2018.00230.
22. Gonzalez, C., & Rizzoli, P. (2018). Landcover-dependent assessment of the relative height accuracy in TanDEM-X DEM Products. *IEEE Geoscience and Remote Sensing Letters,* 15, 1892–1896. doi:10.1109/LGRS.2018.2864774.
23. González-Moradas, M. d. R., & Viveen, W. (2020). Evaluation of ASTER GDEM2, SRTMv3.0, ALOS AW3D30 and TanDEM-X DEMs for the Peruvian Andes against highly accurate GNSS ground control points and geomorphological-hydrological metrics. *Remote Sensing of Environment,* 237, 111509. doi:10.1016/j.rse.2019.111509.
24. Grohmann, C. H. (2018). Evaluation of TanDEM-X DEMs on selected Brazilian sites: comparison with SRTM, ASTERGDEM and ALOS AW3D30. *Remote Sensing of Environment,* 212, 121–133. doi:10.1016/j.rse.2018.04.043.
25. Guth, P. L., & Geoffroy, T. M. (2021). LiDAR point cloud and ICESat-2 evaluation of 1 second global digital elevation models: Copernicus wins. *Transactions in GIS,* 25, 2245–2261. doi:10.1111/tgis.12825.
26. Guth, P. L., Van Niekerk, A., Grohmann, C. H., Muller, J.-P., Hawker, L., Florinsky, I. V., Gesch, D., et al. (2021). Digital elevation models: terminology and definitions. *Remote Sensing,* 13, 3581. doi:10.3390/rs13183581.
27. Heath, D. C., Wald, D. J., Worden, C. B., Thompson, E. M., & Smoczyk, G. M. (2020). A global hybrid VS30 Map with a topographic slope–based default and regional map insets. *Earthquake Spectra,* 36, 1570–1584. doi: 10.1177/8755293020911137.
28. Hengl, T., & Reuter, H. I. (Eds.) (2009). *Geomorphometry: concepts, software, applications*. Amsterdam, the Netherlands: Elsevier.

29. Hijmans, R. J., Bivand, R., van Etten, J., Forner, K., Ooms, J., & Pebesma, E. (2022). *Terra: spatial data analysis. Version 1.5-21*. https://CRAN.R-project.org/package=terra.
30. Hiller, J. K., & Smith, M. (2008). Residual relief separation: digital elevation model enhancement for geomorphological mapping. *Earth Surface Processes and Landforms,* 33, 2266–2276. doi:10.1002/esp.1659.
31. Isaaks, E. H., & Srivastava, R. M. (1989). *Applied geostatistics*. London, UK: Oxford University Press.
32. Jain, A. O., Thaker, T., Chaurasia, A., Patel, P., & Singh, A. K. (2018). Vertical accuracy evaluation of SRTM-GL1, GDEM-V2, AW3D30 and CartoDEM-V3.1 of 30-m resolution with dual frequency GNSS for Lower Tapi Basin India. *Geocarto International,* 33, 1237–1256. doi:10.1080/10106049.2017.1343392.
33. JAXA (2021a). *ALOS global digital surface model "ALOS World 3D – 30m" (AW3D30)*. Tsukuba, Japan: JAXA, http://www.eorc.jaxa.jp/ALOS/en/aw3d30/.
34. JAXA 2021b. *ALOS global digital surface model (DSM) ALOS World 3D-30m (AW3D30) Version 3.2/3.1. 2021. Product description edition 1.2.* Tsukuba, Japan: JAXA EORC.
35. Kakavas, M., Kyriou, A., & Nikolakopoulos, K. G. (2020). Assessment of freely available DSMs for landslide-rockfalls studies. *Proceedings of SPIE,* 11534, 115340R. doi:10.1117/12.2573604.
36. Li, H., & Zhao, J. (2018). Evaluation of the newly released worldwide AW3D30 DEM over typical landforms of China using two global DEMs and ICESat/GLAS Data. *IEEE Journal of Selected Topics in Applied Earth Observations and Remote Sensing,* 11, 4430–4440. doi:10.1109/JSTARS.2018.2874361.
37. Liu, K., Song, C., Ke, L., Jiang, L., Pan, Y., & Ma, R. (2019). Global open-access DEM performances in Earth's most rugged region high mountain asia: a multi-level assessment. *Geomorphology,* 338, 16–26. doi:10.1016/j.geomorph.2019.04.012.
38. Melelli, L. (2014). Geodiversity: a new quantitative index for natural protected areas enhancement. *Geojournal of Tourism and Geosites,* 13, 27–37.
39. Mesa-Mingorance, J.L.; Ariza-López, F.J., (2020). Accuracy Assessment of Digital Elevation Models (DEMs): A Critical Review of Practices of the Past Three Decades. Remote Sens., 12, 2630. https://doi.org/10.3390/rs12162630
40. Minár, J., Krcho, J., & Evans, I. S. (2016). Geomorphometry: quantitative land-surface analysis. In *Reference Module in Earth Systems and Environmental Sciences*, edited by Elias, S. A. Amsterdam, the Netherlands: Elsevier. doi:10.1016/B978-0-12-409548-9.10260-X.
41. Mudd, S. M. (2020). Topographic data from satellites. *Developments in Earth Surface Processes,* 23, 91–128. doi:10.1016/B978-0-444-64177-9.00004-7.
42. Meena, S. R., & Nachappa, T. G. (2019). Impact of spatial resolution of digital elevation model on landslide susceptibility mapping: a case study in Kullu Valley, Himalayas. *Geosciences,* 9, 360. doi:10.3390/geosciences9080360.Pavlis, N.K., Holmes, S.A., Kenyon, S.C., & Factor, J.K. (2012) The development and evaluation of the Earth Gravitational Model 2008 (EGM2008). *Journal of Geophysical Research: Solid Earth*, 117, B04406. doi:10.1029/2011JB008916.

43. Polidori, L.; El Hage, (2020). M. Digital Elevation Model Quality Assessment Methods: A Critical Review. Remote Sens., 12, 3 https://doi.org/10.3390/rs12213522
44. Portale geocartografico (2016). *Lidar*. Trento, Italy: Sistema Informativo Ambientale e Territoriale, Provincia Autonoma di Trento, http://www.territorio.provincia.tn.it/portal/server.pt/community/lidar/.
45. Purinton, B., & Bookhagen, B. (2017). Validation of digital elevation models (DEMs) and comparison of geomorphic metrics on the Southern Central Andean Plateau. *Earth Surface Dynamics,* 5, 211–237. doi:10.5194/esurf-5-211-2017.
46. R Foundation. (2022). *The R project for statistical computing*. Vienna, Austria: R Foundation. https://www.R-project.org/.
47. Rizzoli, P., Martone, M., Gonzalez, C., Wecklich, C., Borla Tridon, D., Bräutigam, B., Bachmann, M., et al. (2017). Generation and performance assessment of the global TanDEM-X digital elevation model. *ISPRS Journal of Photogrammetry and Remote Sensing,* 132, 119–139. doi:10.1016/j.isprsjprs.2017.08.008.
48. Schumann, G. J.-P., & Bates,P. D. (2018). The need for a high-accuracy, open-access global DEM. *Frontiers in Earth Science,* 6, 225. doi:10.3389/feart.2018.00225.
49. Strobl, P. (2020). The new Copernicus digital elevation model. *GSICS Quarterly,* 14, 1, 17–18.
50. Strobl, P. A., Bielski, C., Guth, P. L., Grohmann, C. H., Muller, J.-P., López-Vázquez, C., Gesch, D. B., Amatulli, G., Riazanoff, S., & Carabajal, C. (2021). The digital elevation model intercomparison experiment DEMIX, a community-based approach at global DEM benchmarking. *International Archives of the Photogrammetry, Remote Sensing and Spatial Information Sciences,* XLIII-B4-2021, 395–400. doi:10.5194/isprs-archives-XLIII-B4-2021-395-2021.
51. Tadono, T., Nagai, H., Ishida, H., Oda, F., Naito, S., Minakawa, K., & Iwamoto, H. (2016). Generation of the 30 m-mesh global digital surface model by ALOS PRISM. *International Archives of the Photogrammetry, Remote Sensing and Spatial Information Sciences,* 41, B4, 157–162. doi:10.5194/isprsarchives-XLI-B4-157-2016.
52. Takaku, J., Tadono, T., Tsutsui, K., & Ichikawa, M. (2016). Validation of 'AW3D' global DSM generated from ALOS PRISM. *ISPRS Annals of the Photogrammetry, Remote Sensing and Spatial Information Sciences*, 3, 4, 25–31. doi:10.5194/isprsannals-III-4-25-2016.
53. Takaku, J., & Tadono, T. (2017). Quality updates of 'AW3D' global DSM generated from ALOS PRISM. In *2017 IEEE International Geoscience and Remote Sensing Symposium (IGARSS)*, *Fort Worth, TX, USA, 23-28 July 2017*. doi:10.1109/IGARSS.2017.8128293.
54. Thompson, E. M., Wald, D. J., & Worden, C. B. (2014). A VS30 map for California with geologic and topographic constraints. *Bulletin of the Seismological Society of America* 104 (5), 2313–2321. doi:10.1785/0120130312.
55. Titti, G., Borgatti, L., Zou, Q., Cui, P., & Pasuto, A. (2021). Landslide susceptibility in the belt and road countries: continental step of a multi-scale approach. *Environmental Earth Sciences,* 80, 630. doi:10.1007/s12665-021-09910-1.

56. Trevisani, S., & Florinsky, I. V. (2021). Morphometry. In *Encyclopedia of Mathematical Geosciences*, edited by Sagar, B. S. D., Cheng, Q., McKinley, J., & Agterberg, F. Cham, Switzerland: Springer Nature. doi:10.1007/978-3-030-26050-7_216-1.
57. Trevisani, S., & Cavalli, M. (2016). Topography-based flow-directional roughness: potential and challenges. *Earth Surface Dynamics,* 4, 343–358. doi:10.5194/esurf-4-343-2016.
58. Trevisani, S., & Rocca, M. (2015). MAD: robust image texture analysis for applications in high resolution geomorphometry. *Computers and Geosciences,* 81, 78–92. doi:10.1016/j.cageo.2015.04.003.
59. Trevisani, S., Cavalli, M., & Marchi, L. (2012). Surface texture analysis of a high-resolution DTM: interpreting an Alpine basin. *Geomorphology,* 161–162, 26–39. doi:10.1016/j.geomorph.2012.03.031.
60. Trevisani, S., Pettenati, F., Paudyal, S., & Sandron, D. (2021). Mapping long-period soil resonances in the Kathmandu Basin using microtremors. *Environmental Earth Sciences,* 80, 265. doi:10.1007/s12665-021-09532-7.
61. Trevisani, Sebastiano and Teza, Giordano and Guth, Peter, A Simplified Geostatistical Approach for Characterizing Key Aspects of Short-Range Roughness. Available at SSRN: https://ssrn.com/abstract=4223135 or http://dx.doi.org/10.2139/ssrn.4223135.
62. Servizio catasto di Trento (2011). *Servizio catasto di Trento versione 2.1.5*. Trento, Italy: Ufficio Geodetico, Provincia di Trento, www.mobilekat.provincia.tn.it.
63. Vassilaki, D. I., & Stamos, A. A. (2020). TanDEM-X DEM: comparative performance review employing LIDAR Data and DSMs. *ISPRS Journal of Photogrammetry and Remote Sensing,* 160, 33–50. doi:10.1016/j.isprsjprs.2019.11.015.
64. Wald, D. J., & Allen, T. I. (2007). Topographic slope as a proxy for seismic site conditions and amplification. *Bulletin of the Seismological Society of America,* 97, 1379–1395. doi:10.1785/0120060267.
65. Wang, Z., Bovik, A. C., Sheikh, H. R., & Simoncelli, E. P. (2004). Image quality assessment: from error visibility to structural similarity. *IEEE Transactions on Image Processing,* 13, 600–612. doi:10.1109/TIP.2003.819861.
66. Wilson, J. P., & Gallant, J. C. (Eds.) (2000). *Terrain analysis: principles and applications*. New York: Wiley.
67. Yamazaki, D., Ikeshima, D., Tawatari, R., Yamaguchi, T., O'Loughlin, F., Neal, J. C., Sampson, C. C., Kanae, S., & Bates, P. D. (2017). A high-accuracy map of global terrain elevations. *Geophysical Research Letters,* 44, 5844–5853. doi:10.1002/2017GL072874.

Figures

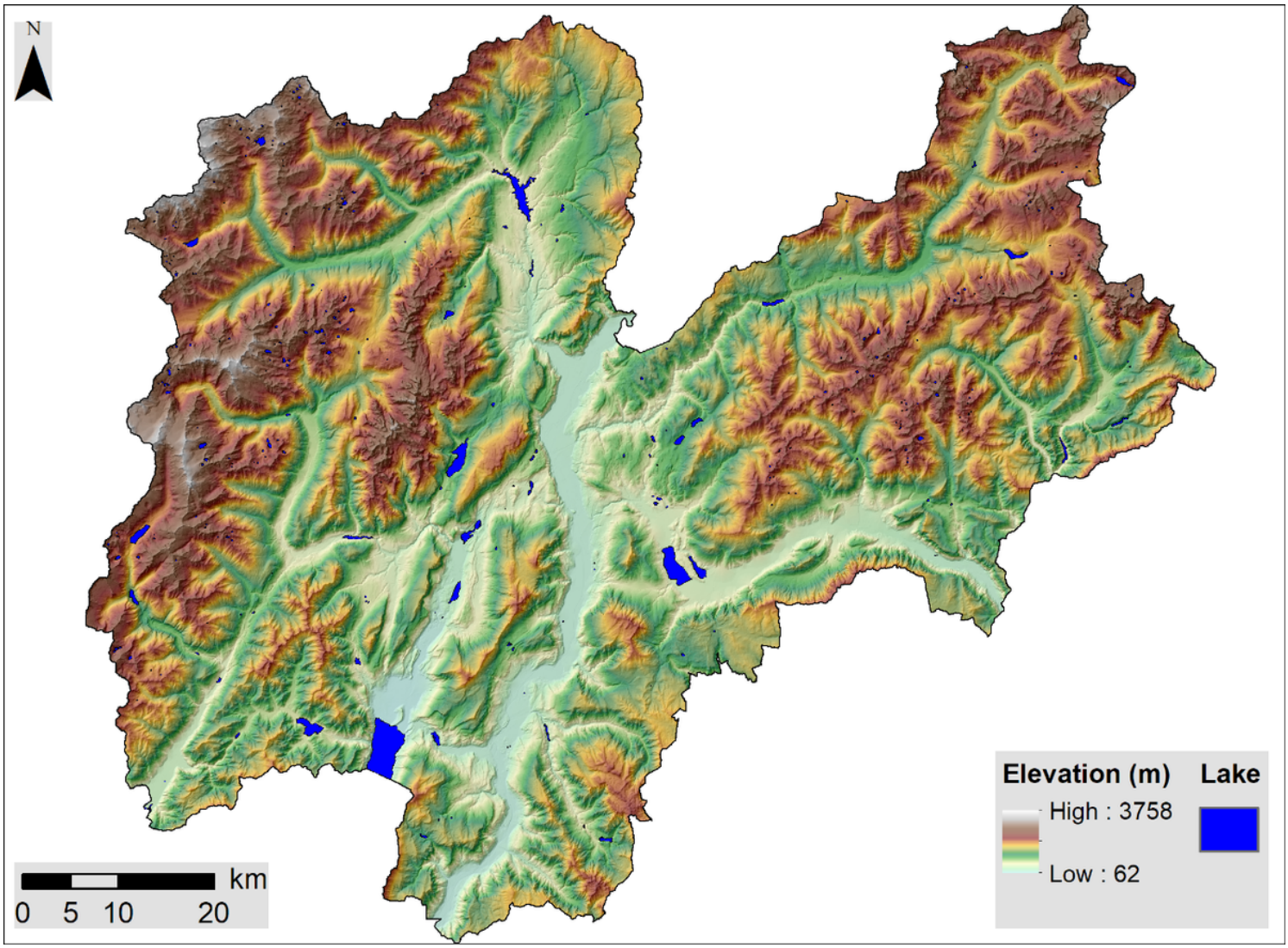

Figure 1

Reference DEM of the Trentino Province at 25 m resolution. The reference DEM has been derived by means of the upscaling of a 2 m resolution airborne Lidar DTM.

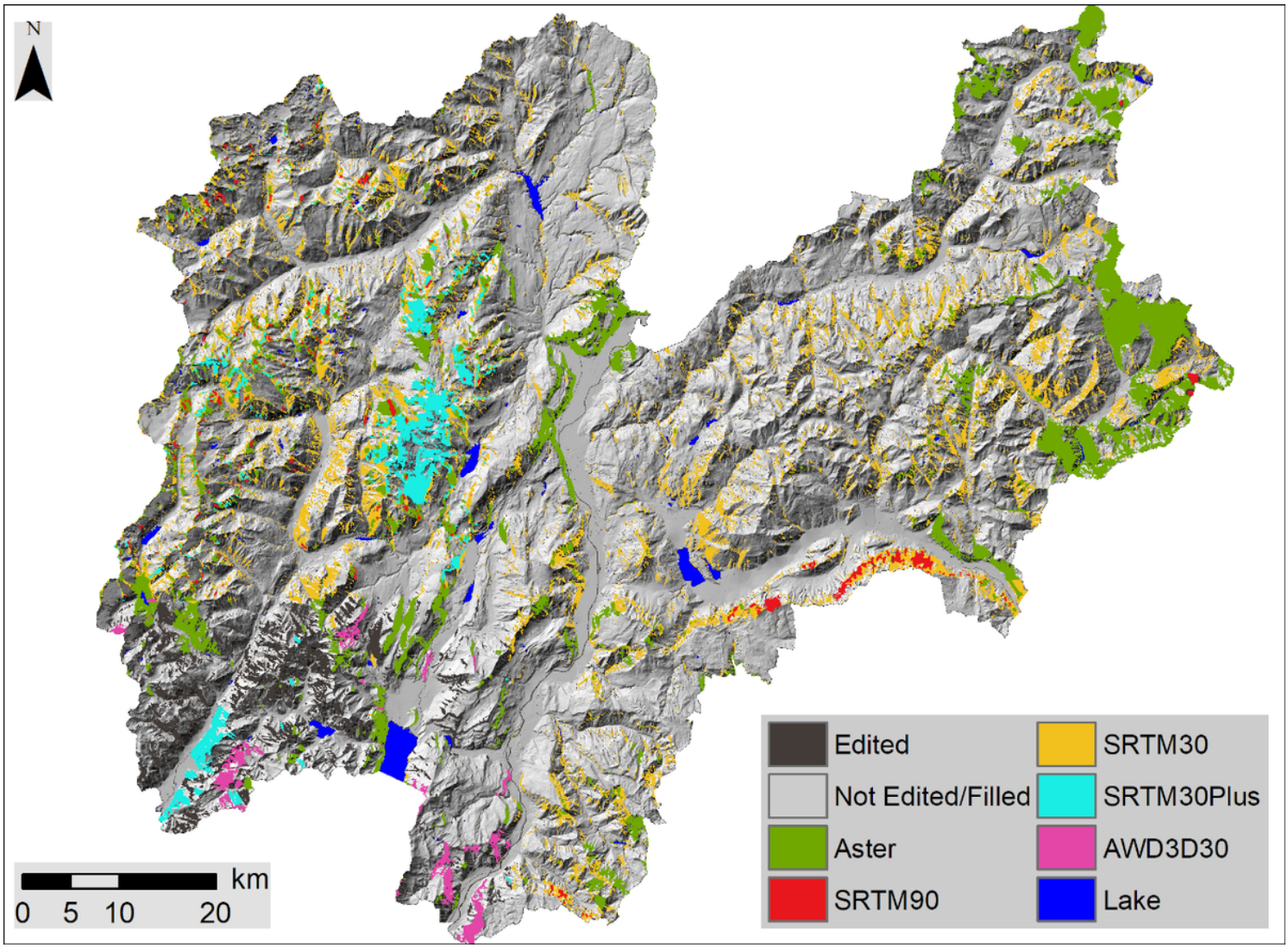

Figure 2

Mask map with void filled areas for the Copernicus DEM, draped on the shaded relief (from reference DEM).

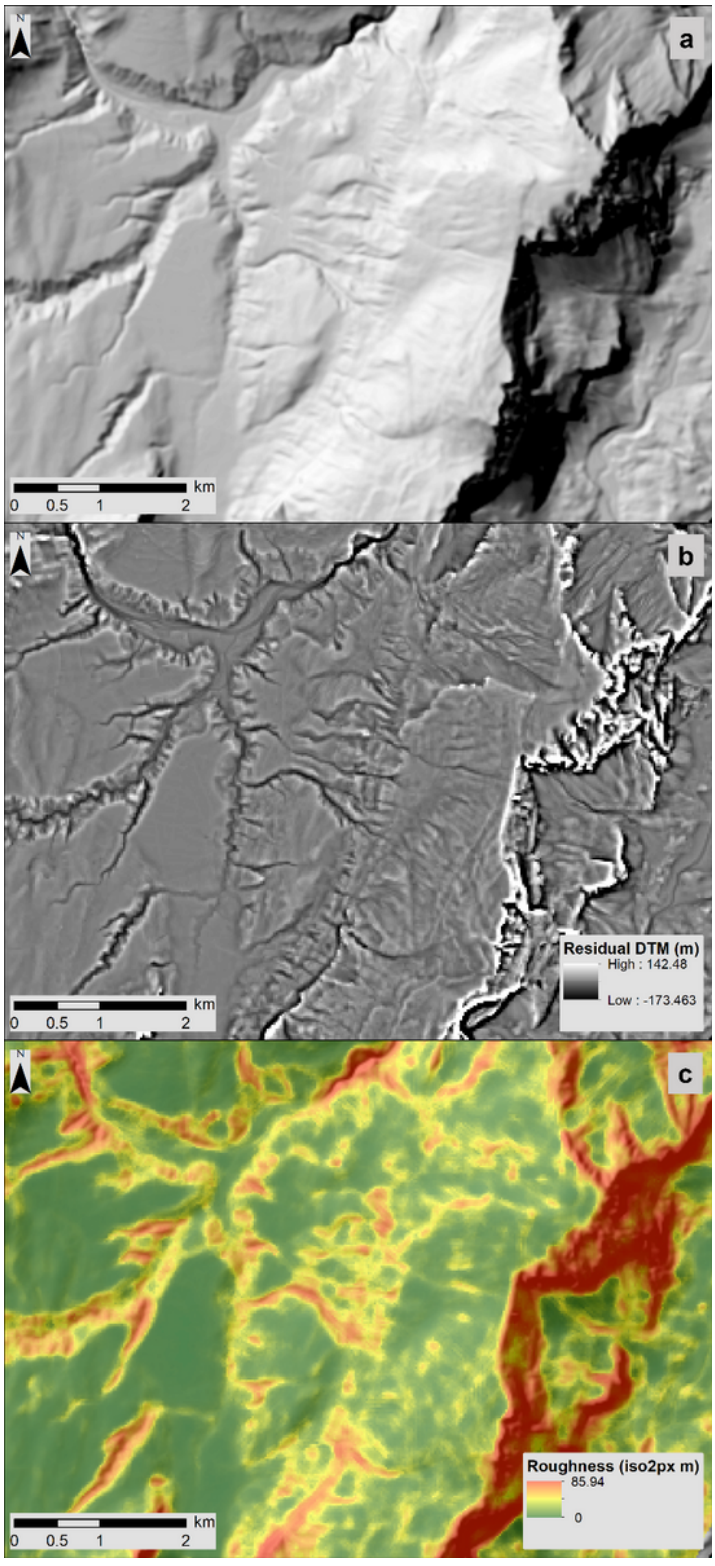

Figure 3

Shaded topography (a) and residual DEM (b) highlighting fine-scale morphology. The residual DEM is the input for calculating local short-range isotropic roughness (lag distance of 2 pixels) represented in (c).

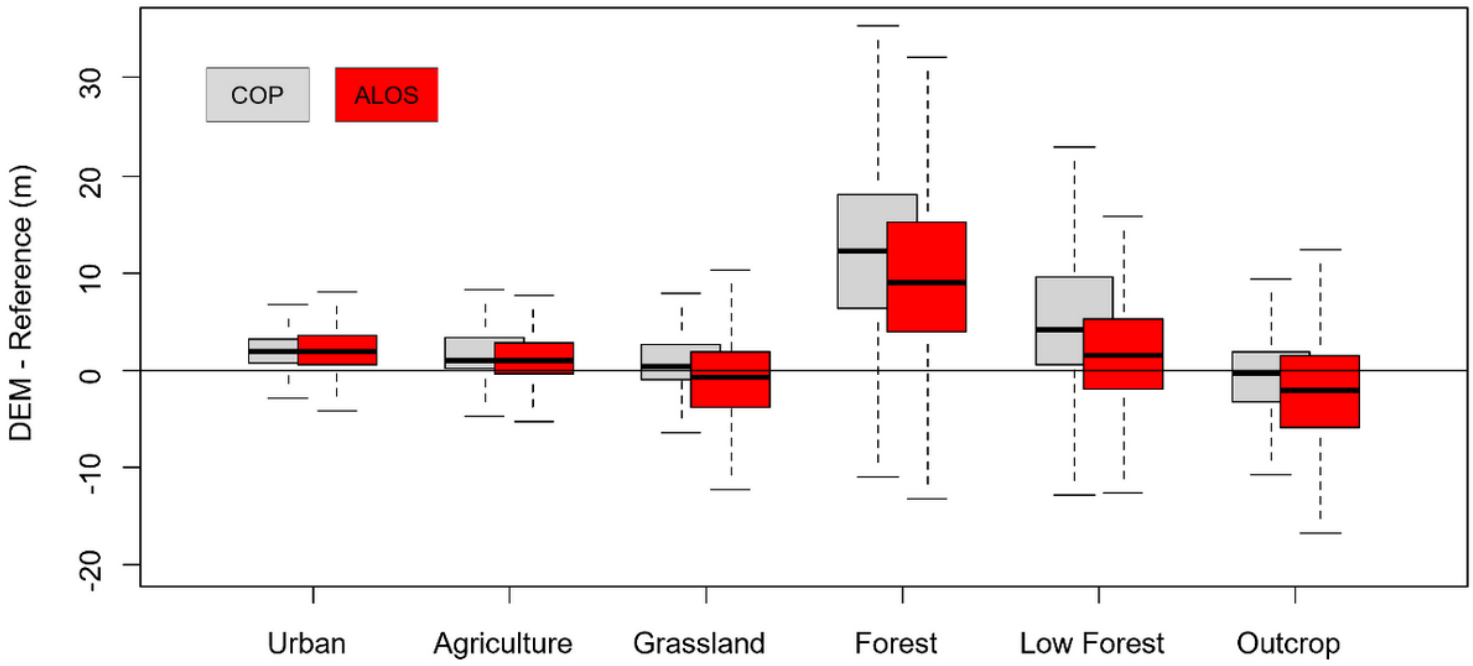

Figure 4

Box plots of the differences between global DEMs and reference in relation to the different land covers.

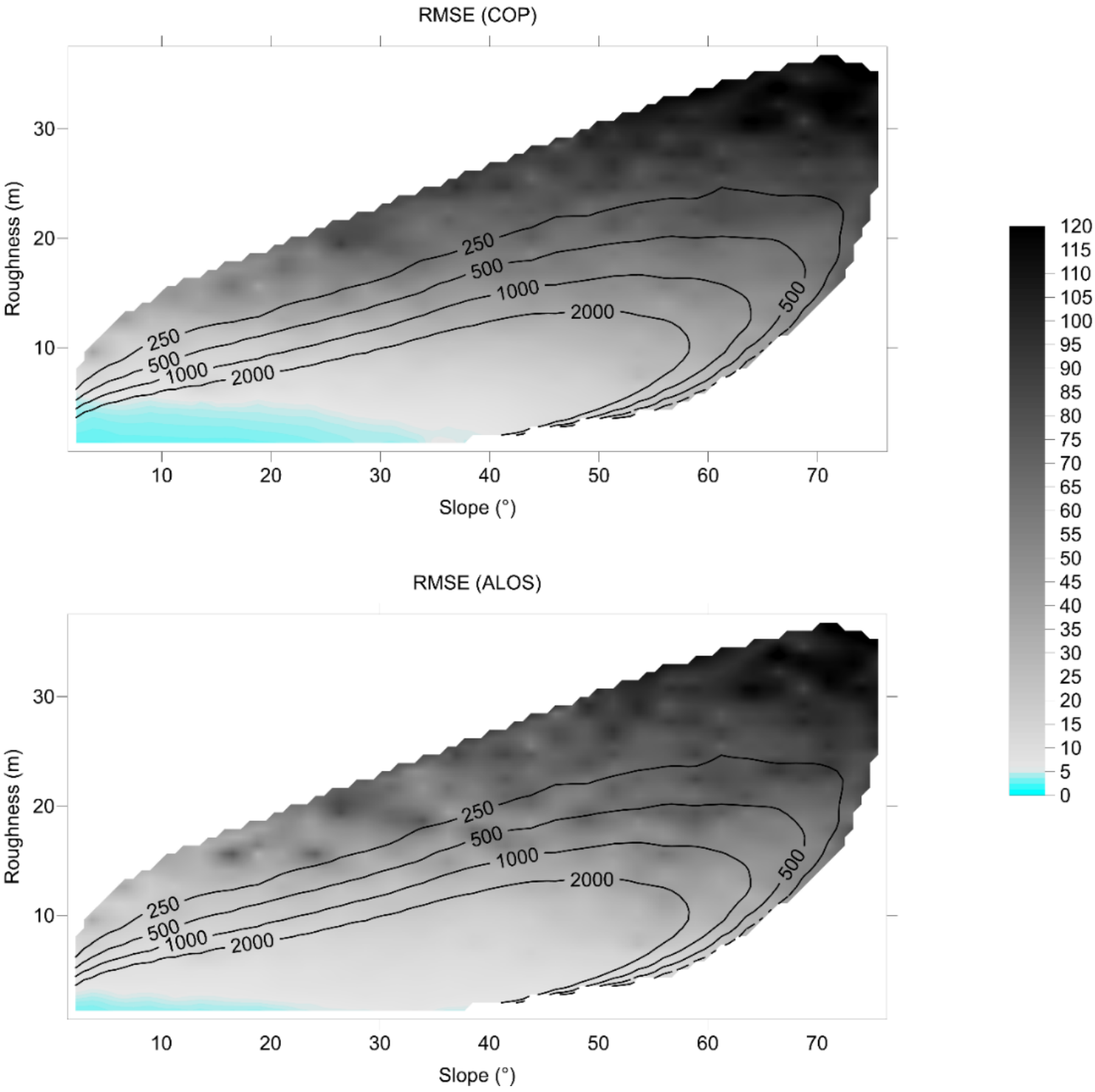

Figure 5

RMSE (m) for COP and ALOS in relation to slope and short-range isotropic roughness considering "Grassland" and "Outcrop" land covers. Contour lines report the number of data used for calculating the RMSE in each class of slope (class interval of 2.5°) and roughness (class interval of 1 m). The values have been interpolated on a regular grid for improving the appearance.

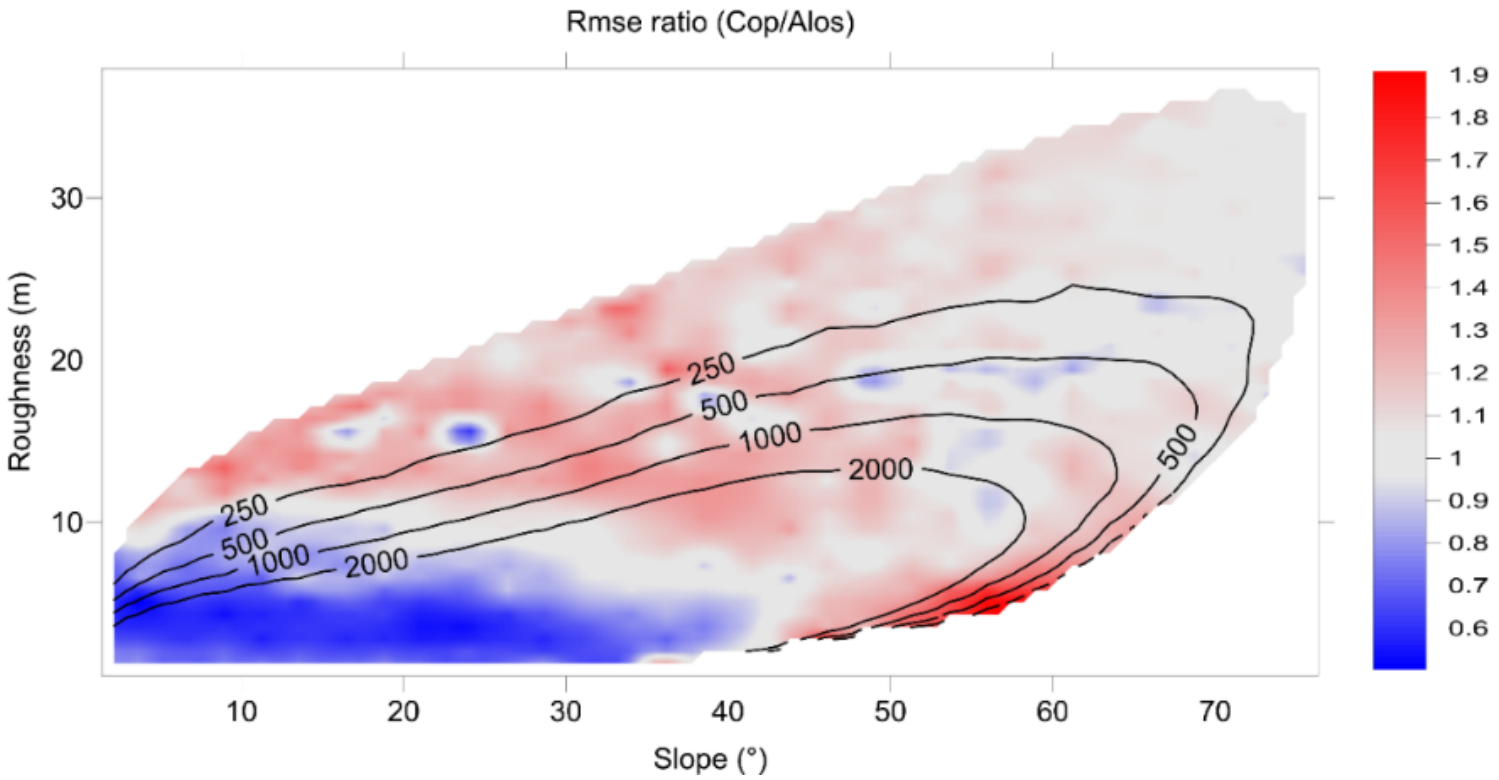

Figure 6

Ratio between the RMSE of COP and ALOS in relation to slope and isotropic short-range roughness considering "Grassland" and "Outcrop" land covers. Contour lines report the number of data used for calculating the RMSE ratio in each class of slope (class interval of 2.5°) and roughness (class interval of 1 m). The values have been interpolated on a regular grid for improving the appearance.

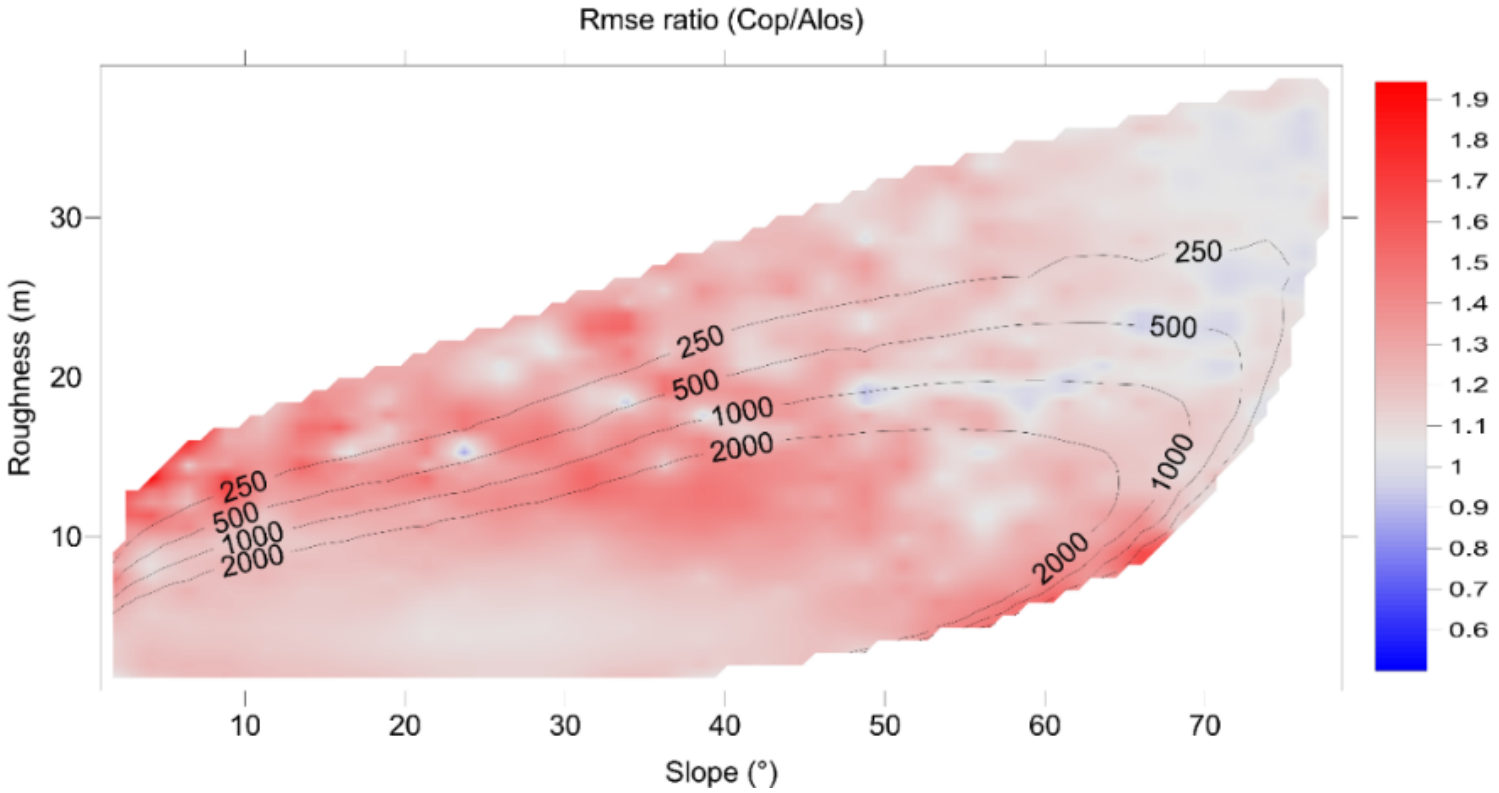

Figure 7

Ratio between RMSE of COP and ALOS in relation to slope and isotropic short-range roughness considering all land covers. Contour lines report the number of data used for calculating the RMSE ratio in each class of slope (class interval of 2.5°) and roughness (class interval of 1 m). The values have been interpolated on a regular grid for improving the appearance.

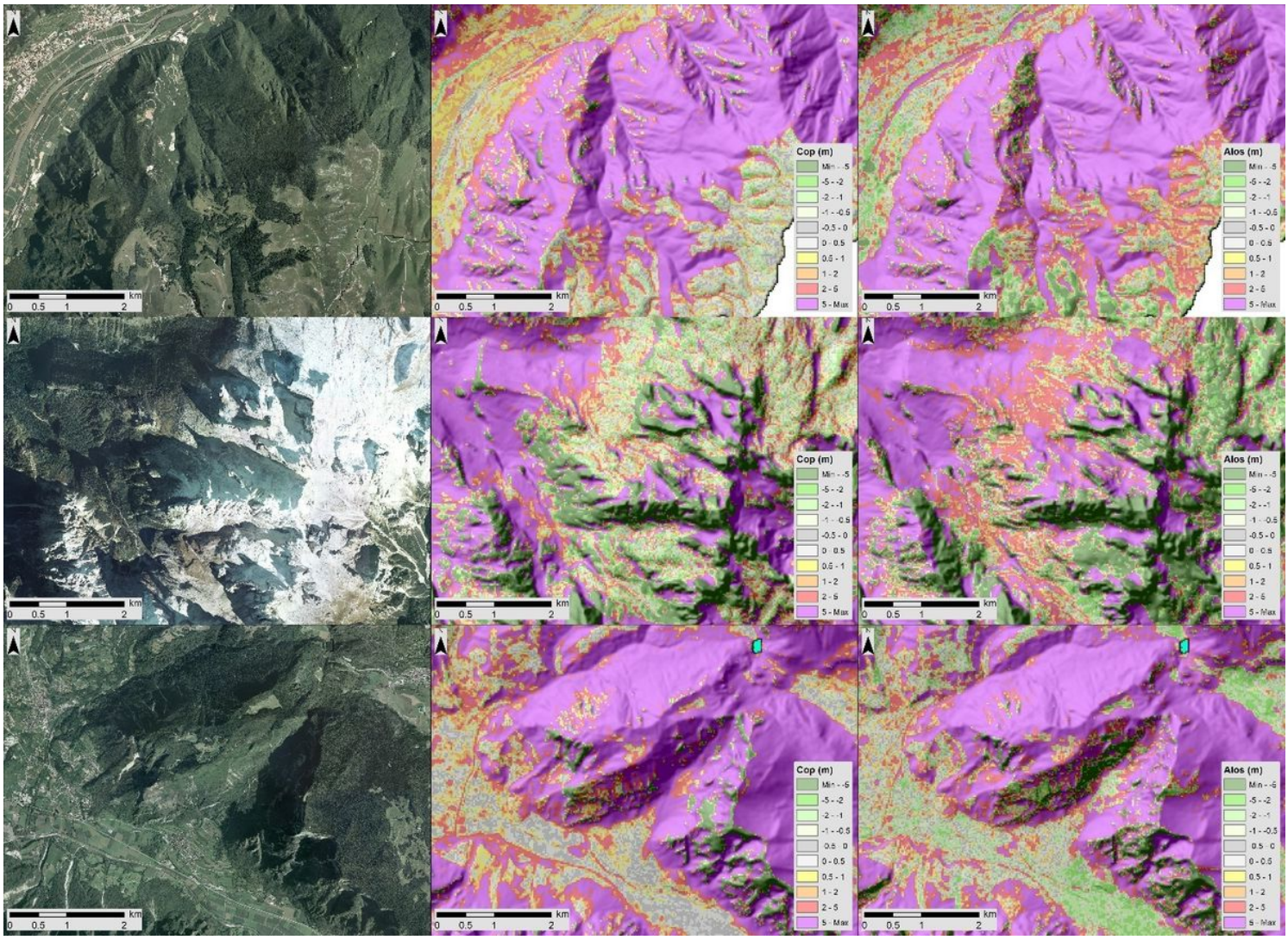

Figure 8

Maps of differences between the global DEMs and the reference (central column COP, left column ALOS).

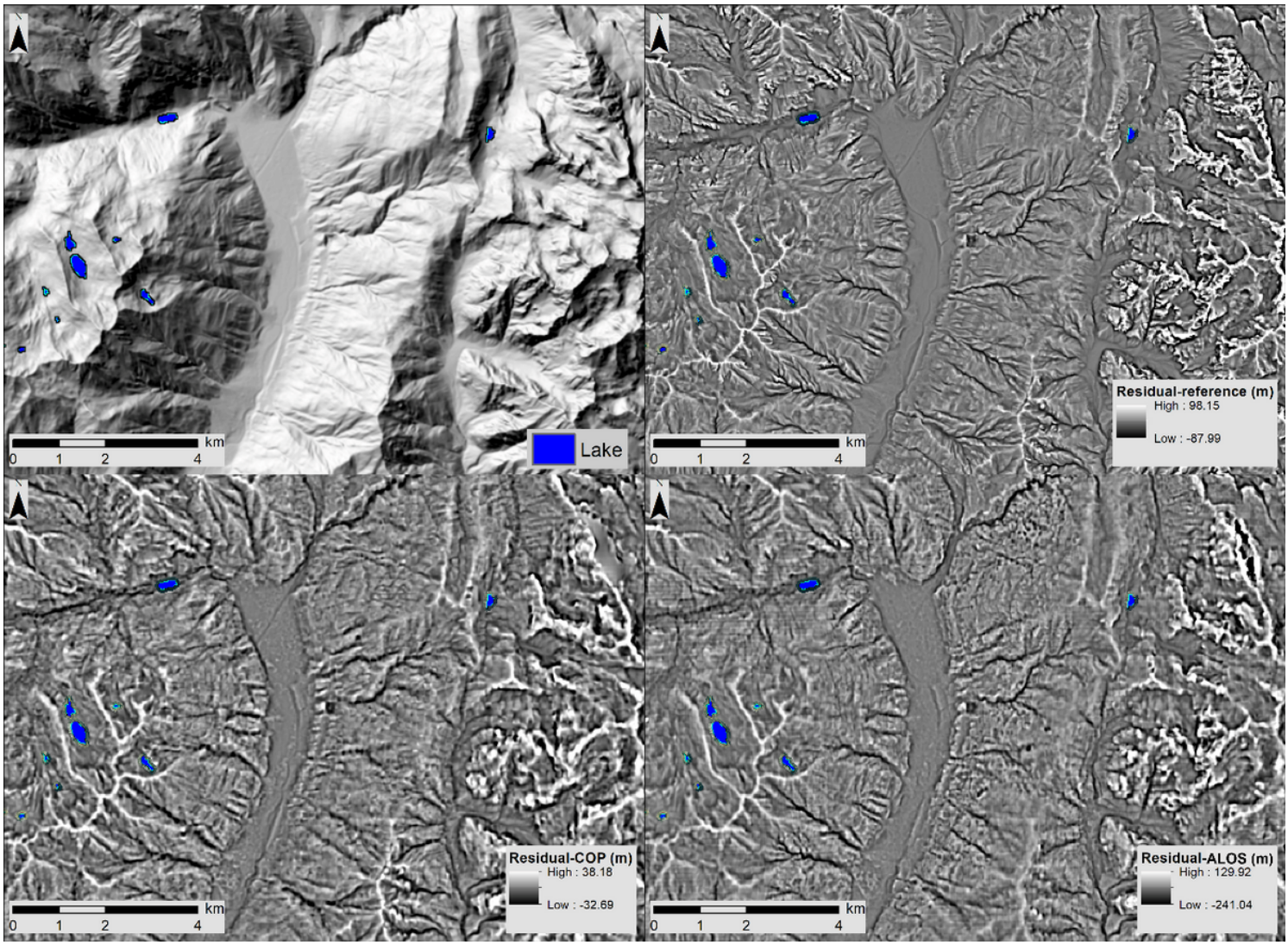

Figure 9

Residual reference DEM and residual global DEMs (COP and ALOS) for an exemplificative area. COP tends to be smoother than ALOS, however ALOS has various artifacts.

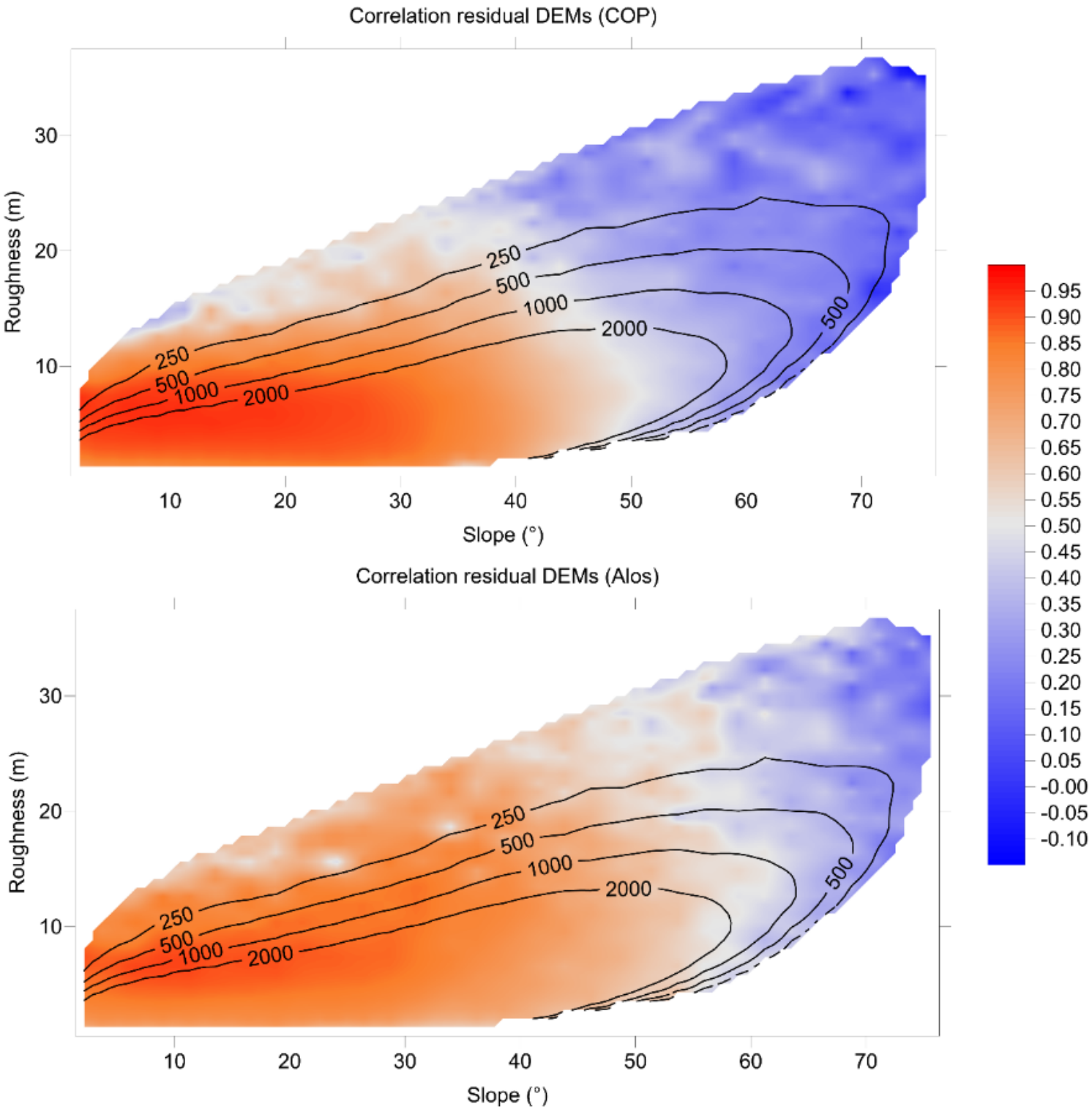

Figure 10

Correlation coefficients between the residual global DEMs and the residual reference DEM in relation to slope and short-range isotropic roughness (lag two pixels) for "Grassland" and "Outcrop" land covers. Contour lines report the number of data used for calculating the correlation in each class of slope (class interval of 2.5°) and roughness (class interval of 1 m). The values have been interpolated on a regular grid for improving the appearance.

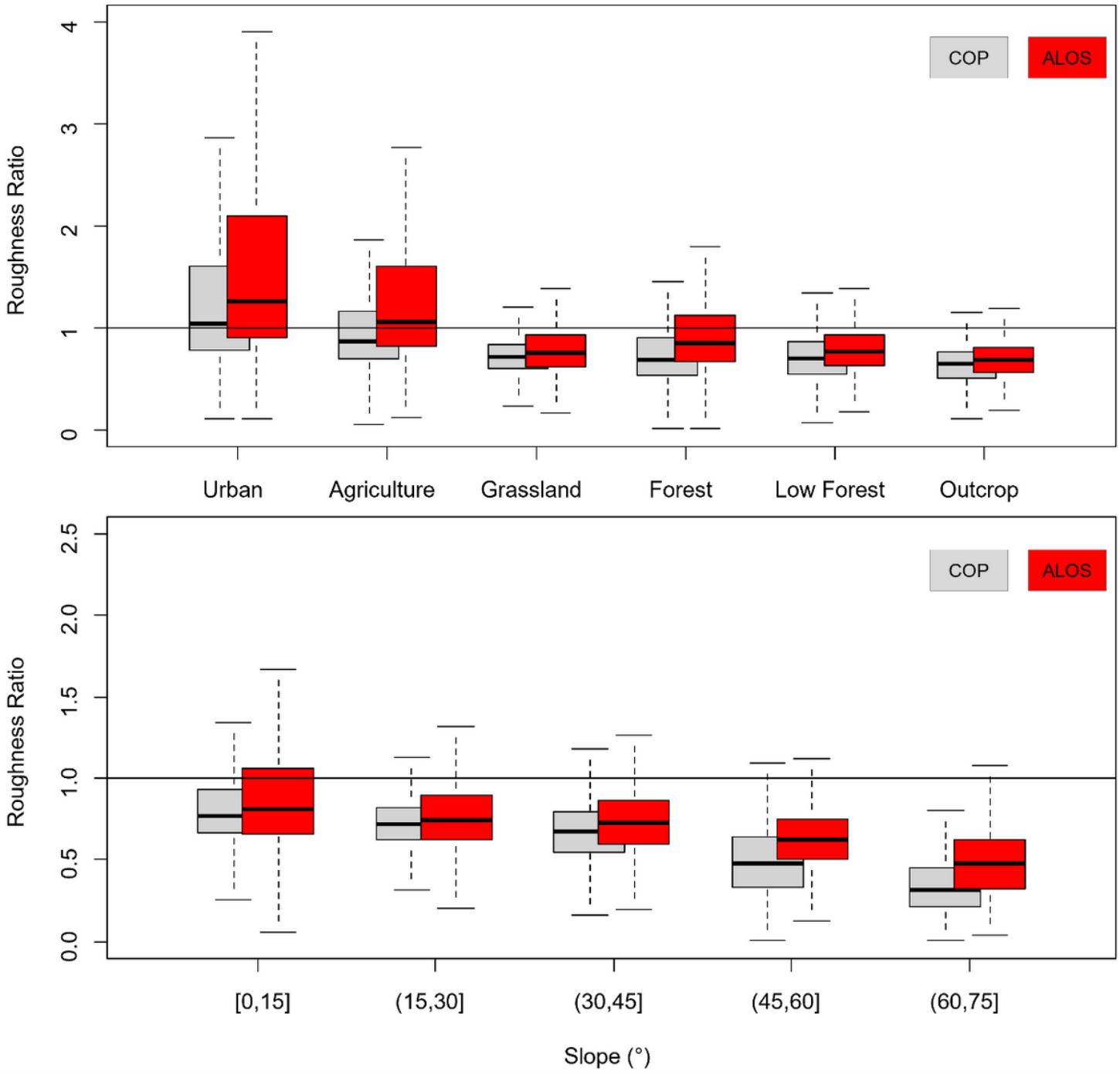

Figure 11

Box plot of the roughness ratios (ratio of global DEM roughness to reference roughness) for COP and ALOS. Top: roughness ratios versus land covers. Bottom: roughness ratios versus slope for "Grassland" and "Outcrop" land covers.

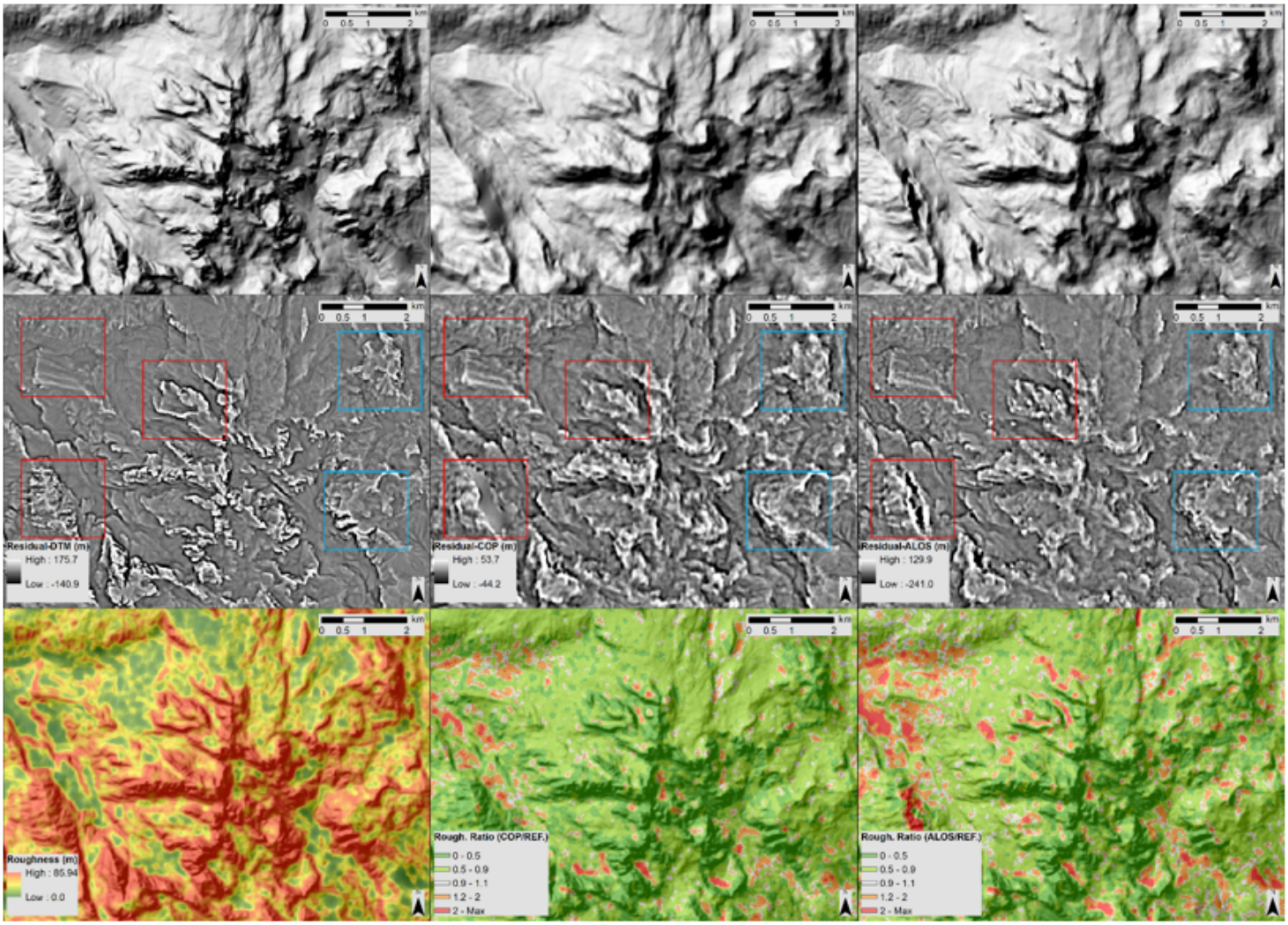

Figure 12

Comparison of the global DEMs fine-scale morphology and short-range roughness with the reference DEM. First row: shaded relief; second row: residual DEMs; third row: roughness for the reference DEM and roughness ratios (ratio of global DEM roughness to reference roughness). Blue boxes: areas with different levels of smoothing of surface morphology. Red boxes: areas with artifacts and void filling processes.

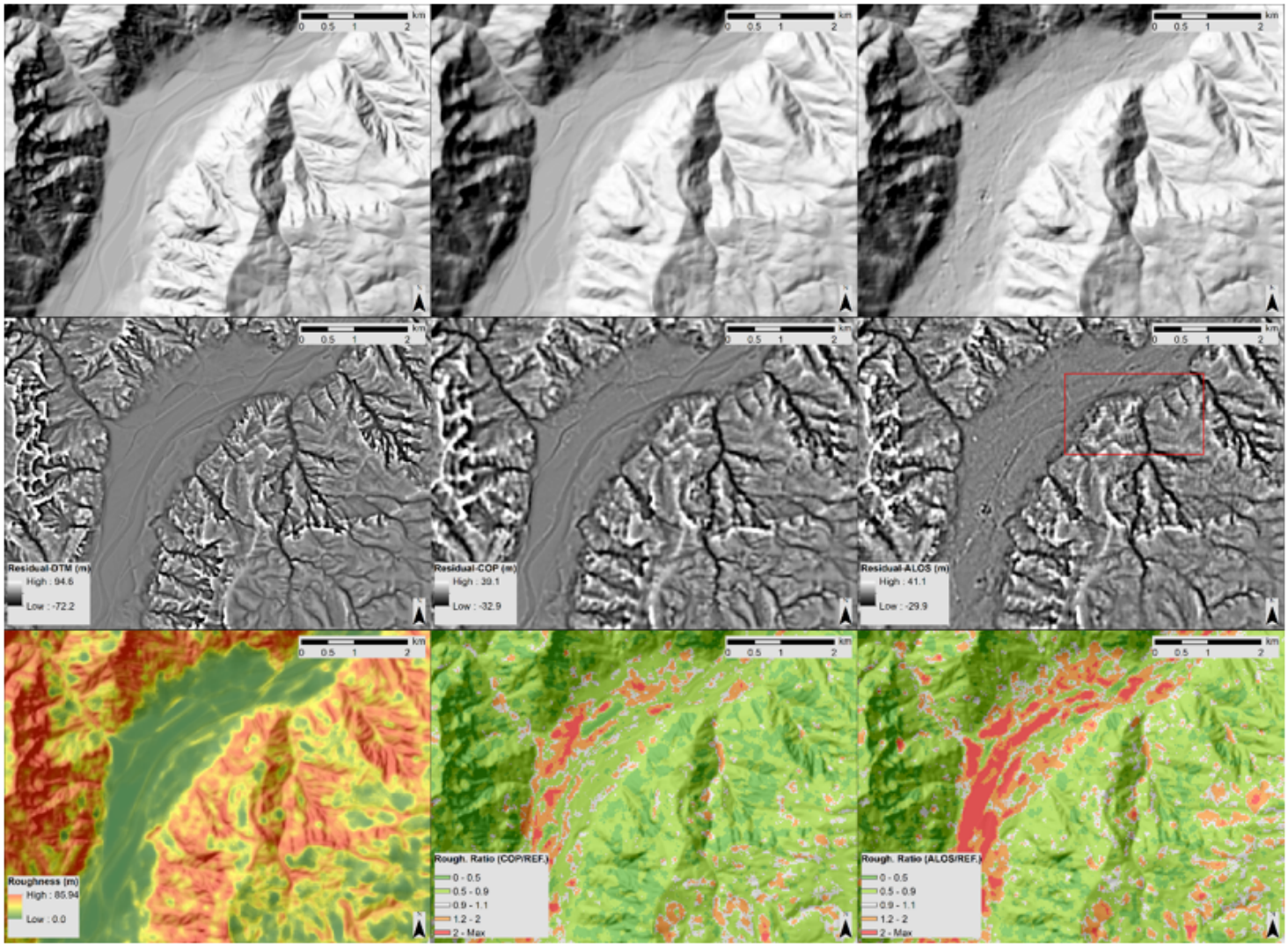

Figure 13

Comparison of the global DEMs fine-scale morphology and short-range roughness with the reference DEM. First row: shaded relief; second row: the residual DEMs; third row: roughness for the reference DEM and roughness ratios (ratio of global DEM roughness to reference roughness). The red box highlights an area with evident artifacts in ALOS.

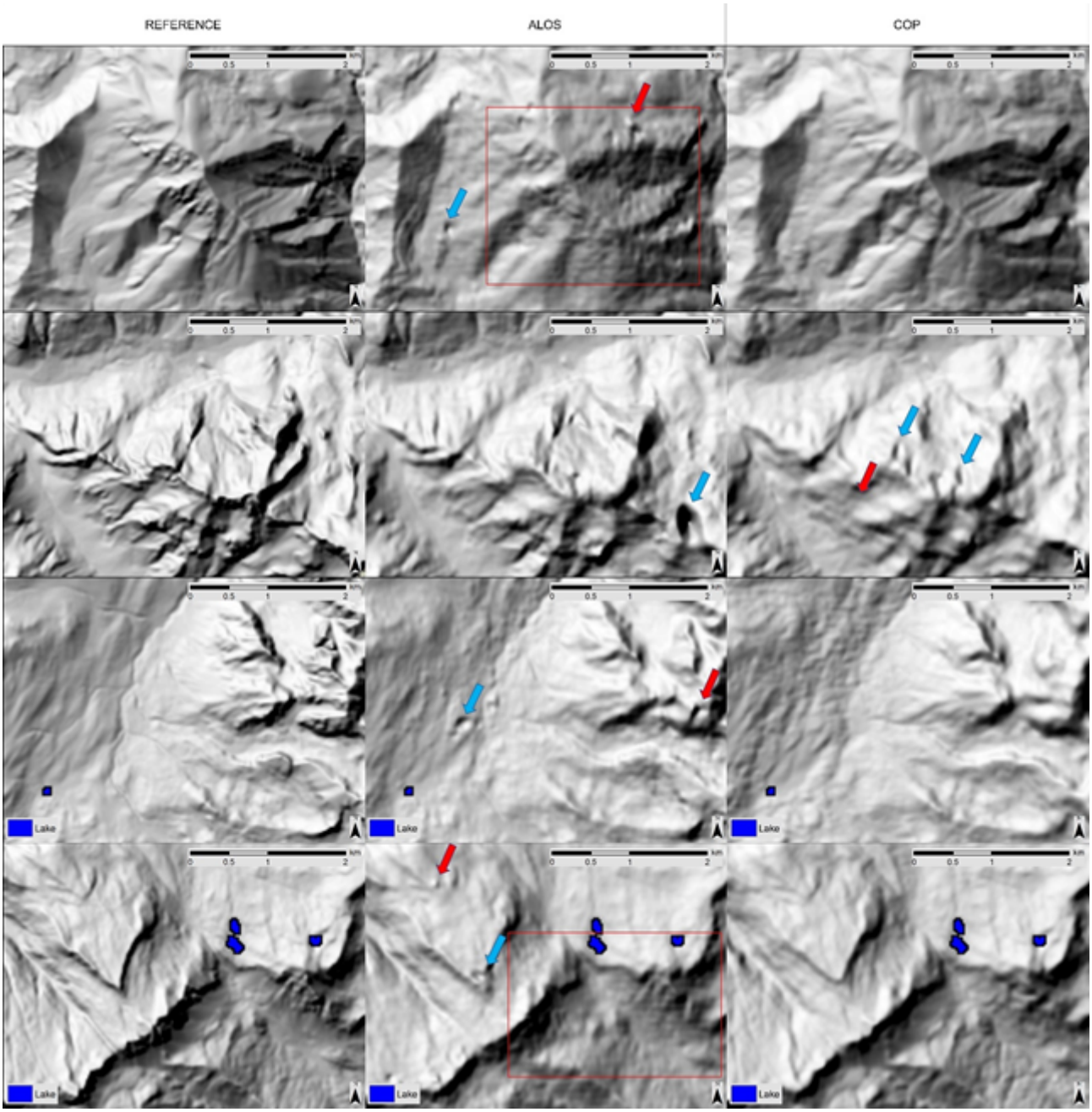

Figure 14

Shaded topography highlighting various artifacts in the ALOS and COP DEMs. Red arrows indicate areas with bumps or filled depressions; blue arrows indicate areas with artificial depressions; the red areas indicate the diffuse presence of artifacts.